J Biomol NMR (2012) 52:151–158
DOI 10.1007/s10858-011-9593-2

ARTICLE

Backbone assignment of perdeuterated proteins using long-range H/C-dipolar transfers

Rasmus Linser

Received: 20 August 2011 / Accepted: 29 November 2011 / Published online: 14 December 2011

Abstract For micro-crystalline proteins, solid-state nuclear magnetic resonance spectroscopy of perdeuterated samples can provide spectra of unprecedented quality. Apart from allowing to detect sparsely introduced protons and thereby increasing the effective resolution for a series of sophisticated techniques, deuteration can provide extraordinary coherence lifetimes—obtainable for all involved nuclei virtually without decoupling and enabling the use of scalar magnetization transfers. Unfortunately, for fibrillar or membrane-embedded proteins, significantly shorter transverse relaxation times have been encountered as compared to micro-crystalline proteins despite an identical sample preparation, calling for alternative strategies for resonance assignment. In this work we propose an approach towards sequential assignment of perdeuterated proteins based on long-range $^{1}H/^{13}C$ Cross Polarization transfers. This strategy gives rise to H/N-separated correlations involving C^{α}, C^{β}, and CO chemical shifts of both, intra- and interresidual contacts, and thus connecting adjacent residues independent of transverse relaxation times.

Keywords MAS solid-state NMR · Magic angle spinning · Perdeuteration · Proton detection · Backbone assignment · Cross polarization

Introduction

Solid-state nuclear magnetic resonance (NMR) spectroscopy has been employed for structural characterization of solid bio-materials with increasing success and popularity over the last years (Castellani et al. 2002; Petkova et al. 2002; Opella and Marassi 2004; Lange et al. 2006; Cady et al. 2010). Apart from providing the possibility to quantify motion with an atomic resolution, solid-state NMR particularly facilitates structure elucidation of intrinsically unstructured biopolymers, for it does not rely on crystallinity and even gives information about ensembles of different conformations (Paravastu et al. 2008; Wasmer et al. 2008; Nielsen et al. 2009). Whereas micro-crystalline materials can nowadays be characterized in a straightforward way using rather sophisticated experiments for assignment (Franks et al. 2007; Linser et al. 2010b; Linser 2011) and structure calculation (Franks et al. 2008; Schanda et al. 2009; Huber et al. 2011; Linser et al. 2011a), even targeting comparably large proteins (Loquet et al. 2008; Cady et al. 2010), intrinsically unstructured proteins are more difficult to characterize due to spectral overlap, poorly defined resonances, and resulting low signal to noise (Heise et al. 2005; Paravastu et al. 2008).

Generally, the effective resolution in NMR experiments can be enhanced by adding additional spectral dimensions for signal dispersion. Apart from methyl (Agarwal et al.

Electronic supplementary material The online version of this article (doi:10.1007/s10858-011-9593-2) contains supplementary material, which is available to authorized users.

R. Linser (✉)
Analytical Centre, University of New South Wales, Sydney, NSW 2052, Australia
e-mail: rasmus_linser@hms.harvard.edu

R. Linser
School of Chemistry, University of New South Wales, Sydney, NSW 2052, Australia

Present Address:
R. Linser
Department of Biological Chemistry and Molecular Pharmacology, Harvard Medical School, 240 Longwood Av., Boston, MA 02115, USA

2006) or methylene protons (Asami et al. 2010), this is particularly beneficial in the case of proton chemical shifts enabled by sparsely abundant or back-substituted amide protons in perdeuterated samples (Zhou et al. 2007b; Linser et al. 2008; Linser 2011), which can be introduced easily and in a defined way and have a reasonable dispersion given resonance linewidths of down to 20 Hz (McDermott et al. 1992; Chevelkov et al. 2006; Lewandowski et al. 2011). Perdeuteration and usage of proton chemical shifts, particularly for fast magic angle spinning, thus represent an important concept towards assignment and structure in recent solid-state NMR.

For rigid micro-crystalline protein samples that are prepared with a low degree of proton back-substitution, as has been shown to be optimal for detection of amide protons in the direct dimension with highest possible signal to noise (Akbey et al. 2009a), long transverse relaxation times T_2 offer the possibility of using scalar couplings for efficient intra- and interresidual correlation experiments (Linser et al. 2008, 2010a, 2011b; Schanda et al. 2009; Huber et al. 2011). Adding to the dipolar-based triple resonance experiments proposed earlier, (Zhou et al. 2007a, b) by these the range of approaches particularly towards assignment has been significantly increased. Even for a preparation identical to the microcrystalline samples used in the aforementioned studies, however, transverse relaxation times T_2 (i.e. spin echo dephasing times) of intrinsically unstructured or membrane embedded proteins have been found to potentially be shorter due to reduced rigidity (Linser et al. 2011b), severely compromising the use of many strategies proposed for perdeuterated proteins to-date.

In contrast to preparations of ubiquitin (Schanda et al. 2010) or the SH3 domain of α-spectrin (Chevelkov et al. 2006), comparably short transverse relaxation times T_2 can be found in membrane-embedded or intrinsically disordered proteins despite excessive sample deuteration circumventing proton-induced dipolar relaxation. Values for echo $T_2(^{15}N)$ previously obtained for this labelling scheme are 10.0 ± 1.0 and 11.1 ± 2.3 ms for the Outer membrane protein G (OmpG) in protonated and deuterated lipids, respectively, and 13.5 ± 0.2 ms for $A\beta^{1-40}$, versus 21.8 ± 3.3 ms for the SH3 domain. (Linser et al. 2011b) The two latter values were determined using samples doped with 75% $[Cu(edta)]^{2-}$, which has been known not to significantly enhance transverse relaxation. (Linser et al. 2007) The tendency of T_2 for these kinds of targets towards low values provokes the necessity of H/N/C triple-resonance assignment experiments for perdeuterated proteins that are independent of transverse relaxation times T_2. Noteworthy, in contrast to highly flexible protein loops (Siemer et al. 2006), enhanced transverse relaxation in these cases is not linked to abrogation of Cross Polarization, as is obvious from previous studies on the same proteins (Hiller et al. 2005; Paravastu et al. 2008). This urges to engineer pulse schemes based on dipolar magnetization transfers rather than scalar transfers, not only for H/N transfers, as suggested earlier (Linser et al. 2011b), but throughout the whole pulse sequence.

The most obvious dipolar-based H/N/C experiment could employ the basic NCACX (Pauli et al. 2001) approach with an additional preceding incrementation of ^{1}H chemical shifts, however, detection of ^{13}C rather than ^{1}H does not pay respect to the higher gyromagnetic ratio of protons and makes refocusing of homonuclear ^{13}C–^{13}C scalar coupling difficult. For the opposite order, i.e. with a subsequent, direct detection of protons, as proposed earlier (Zhou et al. 2007a, b), we found that the combination of homonuclear mixing and an N/C CP transfer can effectively be replaced by use of long-range C/H transfers (Agarwal et al. 2010; Linser 2011). Due to the high gyromagnetic ratio of the involved nuclei and accordingly strong dipolar interaction, distances of several Å can be traversed without additional ^{13}C homonuclear mixing, enabling more nuclei than those directly bonded to ^{15}N (i.e. intraresidual C^{α} and interresidual CO) to be included into correlation experiments. This is particularly interesting since homonuclear mixing, which would be necessary otherwise for more comprehensive correlations, is less effective in the case of perdeuterated than for protonated proteins (Akbey et al. 2009b; Huang et al. 2011), making experiments for unambiguous sequential assignment with reasonable signal to noise hard to achieve.

In this work, we employ the α-spectrin SH3 domain as a well-understood solid-state NMR standard to develop a purely dipolar-based assignment experiment employing long-range H/C transfers to overcome the shortcomings and sequentially correlate residues close in space by means of their carbonyl, C^{α}, and C^{β} chemical shift with an H/N separation.

Materials and methods

Spectra of the SH3 domain of chicken α-spectrin were recorded using approximately 6 mg of uniformly ^{2}H,^{15}N,^{13}C-labelled protein, which was expressed and purified as described earlier. (Linser et al. 2007) Microcrystallization was pursued in a buffer containing 75% D_2O and 25% H_2O as well as 75 mM $(NH_4)_2[Cu(edta)]$ by pH shift from 3.5 to 7.5. The material was center-packed into a 2.5 mm rotor using compressed Teflon® tape in the bottom and top of the rotor. All NMR experiments were carried out at 700 MHz proton Larmor frequency, 25 kHz MAS, and 25°C effective temperature, using a 2.5 mm triple-resonance probe on a Bruker Avance III spectrometer. CP contact times of 3.5 ms, 280 μs, and 3 ms and effective fields of 85 kHz/

50 kHz (70–100% ramp on ^{1}H), 20 kHz/43 kHz (70–100% ramp on ^{15}N), and 35 kHz/50 kHz (70–100 % ramp on ^{13}C) were used for ^{1}H/^{13}C, ^{1}H/^{15}N, and ^{13}C/^{15}N transfers, respectively. Decoupling fields were set to 4 kHz on ^{15}N and 7 kHz on ^{1}H. Recycle delays were set to 400 ms.

Data processing, chemical shift assignment, read-out of intensities, and preparation of figures was performed using Bruker Topspin, Sparky (Goddard and Kneller 2004), and CcpNmr Analysis software (Vranken et al. 2005).

Results and discussion

Figure 1a represents the contacts obtainable by employing long-range C/H transfers for sequential backbone assignment.

Figure 1b–d present the pulse schemes used for exploiting the correlations enabled by long-range transfers in 2D (Fig 1b) or 3D experiments (Fig. 1c, d), denoted hC$^{\alpha}$H or hCOH (Fig. 1b), hC^{x}hNH (Fig. 1c), and hC$^{\alpha}$hNH or hCOhNH (Fig. 1d) in the following, as based on their transfer pathways. The detour magnetization transfer pathway employed for ^{15}N chemical shift separation of H/C correlations in Fig. 1c and d using back-and-forth transfers between ^{1}H and ^{15}N is justified by two factors. (Linser 2011) On one hand, the transfer efficiency between these nuclei is high (58% as determined from a comparison of a direct excitation ^{1}H experiment and an experiment in which proton start magnetization is transferred to ^{15}N^{H} and back, see Supplementary Figure 1). On the other hand, any N/C transfer, generally yielding low transfer efficiencies and pushing the probehead and sample integrity to their limits, is avoided. Supplementary Figure 2 shows a comparison between a direct H/C transfer and a double CP experiment with a 2-step transfer of ^{1}H magnetization to ^{13}C$^{\alpha}$ via ^{15}N. Using optimized conditions, the latter pathway gives a signal to noise that is weaker than a direct H/C transfer by a factor of 7.3 (reduced to 13.7%) even in the absence of any homonuclear mixing step. This implies a lower loss of magnetization for strategies relying on H/C transfers even when an additional transfer from ^{1}H to ^{15}N and back is added—which induces a 3-fold decrease of the obtained signal (to 33.8%) only. These numbers are according to the bulk signal of ^{13}C$^{\alpha}$ resonances.

In all pulse schemes depicted, polarization of ^{13}C starts out with a COPORADE excitation (Linser 2011). An additional concept to effective ^{13}C polarization via a Triple Resonance CP from ^{1}H and ^{2}H, which could potentially be combined with it, has been proposed recently given a 4-channel probe is available (Akbey et al. 2011). The COPORADE strategy, adding a ^{13}C direct polarization (DP) top-up to the polarization obtained through CP, was found particularly useful for those carbons that are far away from back-substituted amides and residual methyls. In the case that particularly those carbons are of interest, one may choose longer recycle delays than required for CP excitation in order to strengthen the direct polarization component. Using short recycle delays of 0.4 s, we show here, however, that an additional 30% of start magnetization can be obtained even with a recycle delay optimised for ordinary CP (i.e.

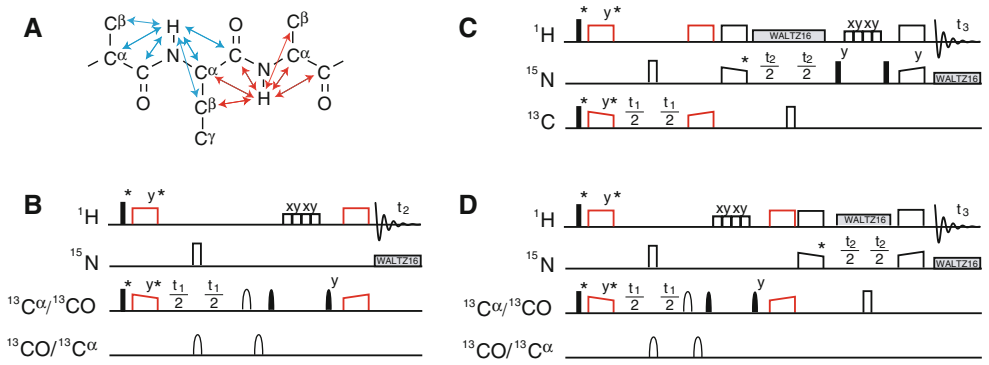

Fig. 1 **a** Magnetization transfer network achieved through long-range H/C Cross Polarization. The distances covered reach up to C$^{\beta}$ in most cases (**b**–**d**). Pulse schemes based on H/C long-range transfers (*red*). **b** 2D H/CO or H/C^{ali} correlation using selective ^{13}C pulses for *J*-refocusing upon incrementation and transfer of either species (hC$^{\alpha}$H/hCOH). **c** 3D triple-resonance correlation using an additional out-and-back transfer to ^{15}N (hC^{x}hNH). Here, ^{1}J(CO/C$^{\alpha}$) is not refocused for encoding of the whole ^{13}C bandwidth with better sensitivity. **d** Similar to **c**, but employing *J*-refocusing for ^{1}J(CO/C$^{\alpha}$), restricting the experiment to either aliphatic or carbonyl correlations (hC$^{\alpha}$hNH/hCOhNH). In each case an additional start magnetization on ^{13}C is achieved by adding direct polarization by means of COPORADE excitation (Linser 2011). *Filled* and *open bars* represent 90° and 180° pulses, *rounded bars* annotate soft rectangular and G3 shaped pulses (Emsley and Bodenhausen 1990) when applied on or of-resonance, respectively. *Asterisks* denote pulses phase shifted according to TPPI for phase-sensitive correlations. CP transfers in *red* (H/C long-range transfers) employ 3–4 ms contact. *Shorter bars* on ^{1}H reflect 2,000 µs water purge pulses with an effective field of 10 kHz. See the "Materials and methods" section for additional parameters

according to ^{1}H T_1) and for carbons closer to the H^N. Figure 2 shows a comparison between hC^{x}hNH experiments recorded using COPORADE, CP only, and DP only for excitation under these conditions. Supplementary Figure 3 shows the carbon resolved benefits of COPORADE.

Similar to ^{15}N steady-state magnetization contributing additional 10% to the signal of TROSY experiments in solution NMR, (Pervushin et al. 1998) we propose that this add-up should be incorporated routinely into other, traditional pulse schemes as well, as small gains in s/n at no cost are also found for protonated samples and without paramagnetic doping (data not shown), particularly for ^{13}CO nuclei, for which no directly bound ^{1}H are present (gains on the order of $\sim$10%) or when recycle delays are chosen longer than what would correspond to ^{1}H T_1 in order to maintain sample integrity.

3D hC^{x}hNH correlation experiments can be recorded encoding the full spectral width of carbons, enabling matching of strips with regard to the three involved correlations, CO, C^{α}, and C^{β}. The maximal obtainable resolution in this case is determined predominantly by the non-refocused ^{1}J scalar couplings between carbon nuclei. Whereas this is problematic for sufficient resolution of C^{α} and especially ^{13}CO resonances, given their narrow spectral distribution in comparison to the relatively large value of $^{1}J_{C\alpha CO}$, C^{β} correlations are only affected by smaller $^{1}J_{Cali}$ and, more importantly, have a broader spectral range. A higher signal to noise can be achieved through the omission of selective pulses that would otherwise be needed for refocusing of ^{1}J-couplings, which is beneficial for these correlations weaker in signal to noise due to the larger average distance between back-substituted $^{1}H^N$ and C^{β}. Figure 3 shows the profile of involved spins for the unrefocused version of the experiment. In Fig. 3a and b, the resolution is poor due to short ^{13}C incrementation t_{1max}, resembling an experiment with maximum signal to noise beneficial for C^{β} resonances. Figure 3c shows the carbonyl region with a longer evolution, representing the highest realistic resolution obtainable without refocusing $^{1}J_{C\alpha CO}$.

A better resolution can potentially be achieved by selective inversion through shaped ^{13}C 180° pulses. In order to reduce artefact peaks at 0 frequency, selective (soft rectangular) 90° pulses can be employed and phase cycled in order to suppress the unwanted magnetization pathways (see Figs. 1b, d). Whereas the unrefocused version of the pulse scheme (see Fig. 1c) uses water suppression during transverse ^{15}N magnetization, which is encoded as the last dimension and has generally longer longitudinal relaxation times, the refocused versions of the pulse schemes employ water suppression during longitudinal ^{13}C magnetization.

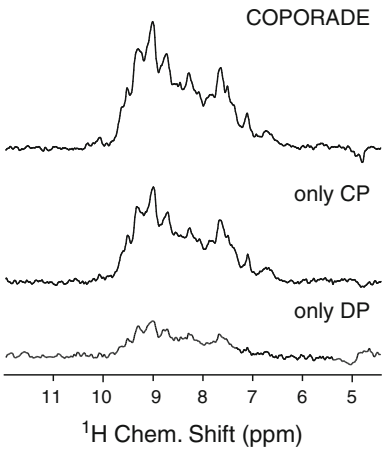

Fig. 2 Add-up of signal to noise by COPORADE excitation (Linser 2011) for short recycle delays and carbon atoms close to the partly protonated backbone. Adding direct polarization in addition to an H/C CP (using COPORADE excitation), the signal to noise is increased by around 30%. The experiments were recorded using the first increment of hC^{x}hNH experiments and 128 scans with a recycle delay of 400 ms, corresponding to approximately 3 × T_1 (^{1}H) and roughly 0.5–0.25 × T_1 (^{13}C) (based on measured T_1 of 800 ms, 1.3 s, and 1.8 s for the bulk aliphatic carbons, carbonyls and C^{α} carbons, respectively)

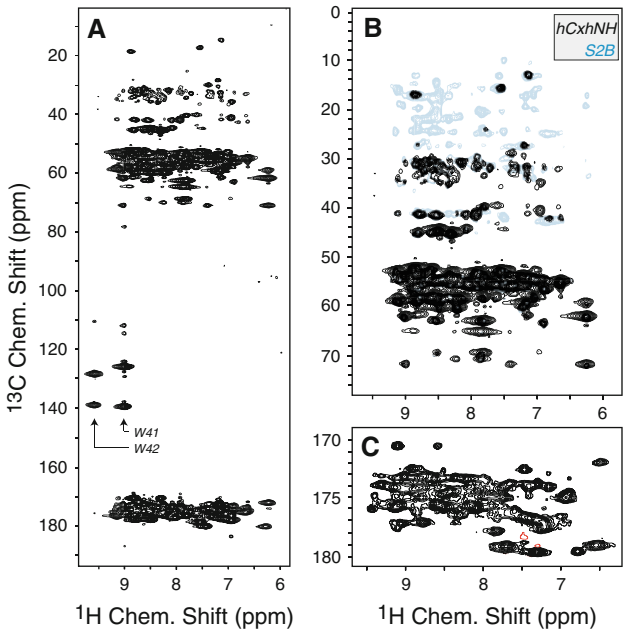

Fig. 3 Distribution of carbon resonances accessed by 3D hC^{x}hNH experiments. **a** Projection of an unrefocused 3D experiment along the ^{15}N dimension (F2). The 3D experiment was acquired over 2.5 d using a t_{1max} of 4 ms for ^{13}C chemical shift encoding and 100 and 35 Hz exponential line broadening for ^{13}C and ^{1}H, respectively. **b** Comparison of the aliphatic resonances accessed here (*black*, as in **a**) with the complete aliphatic set as obtained from an *S2B* experiment (*blue*) recorded as a 2D H/C correlation in this case (Linser 2011). **c** Realistic maximal resolution obtainable without refocusing of $^{1}J_{C\alpha CO}$ (in contrast to Fig. 4a), as obtained in a 2D version of the unrefocused experiment within 3.5 h using a t_{1max} of 12 ms and exponential (25 Hz) and Gaussian multiplication of −10 Hz with a shift of the bell by 0.2 for ^{1}H and ^{13}C, respectively

Although renewed ^{1}H polarization can potentially build up between an early water suppression and detection, this strategy is reasonable due to the fact that no additional (90°) pulses have to be introduced in order to make the scheme selective for either aliphatic or CO coherences this way. Figure 4 shows the benefit of $^{1}J_{C\alpha CO}$ refocusing for the resolution given for the CO-encoded spectrum, using 18 ms t_{1max}. The strategy employed, i.e. a Gaussian G3 pulse (Emsley and Bodenhausen 1990) of 500 µs duration and a second alike pulse for correction of off-resonance

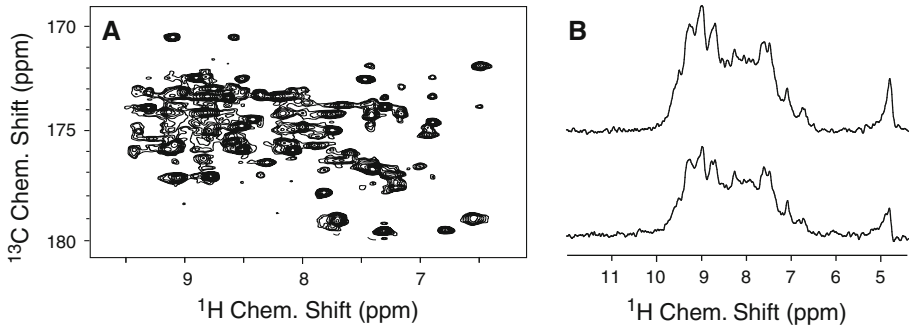

Fig. 4 **a** Resolution in the ^{13}CO dimension upon refocusing of $^{1}J_{C\alpha CO}$ scalar couplings. This spectrum was recorded as a 2D experiment using pulse scheme Fig. 1b with a t_{1max} of 18 ms within 8 h. **b** Refocusing and compensation of off-resonance effects by two shaped G3 pulses (Emsley and Bodenhausen 1990) was found to come at a cost of 31% of the signal to noise

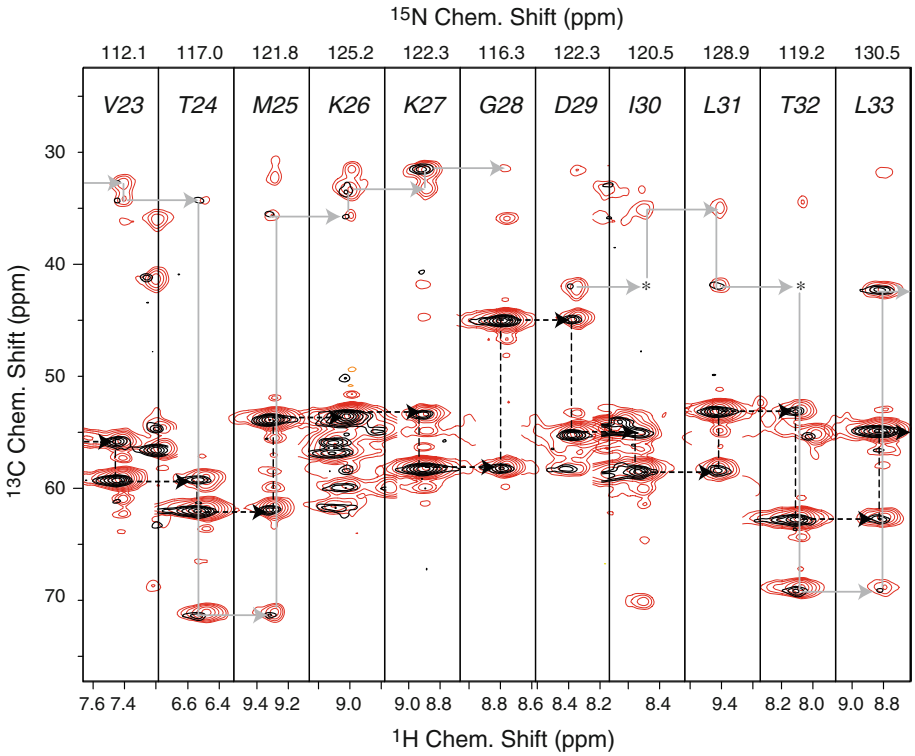

Fig. 5 Aliphatic region of the 3D correlation experiments hC^{x}hNH (unrefocused, *red*, as in Fig. 3) and hC$^{\alpha}$hNH (with refocused homonuclear scalar couplings, shown in *black*). *Arrows* denote the sequential walk along the backbone, *black dashed* ones referring to C$^{\alpha}$ chemical shifts and *grey* ones to C$^{\beta}$ chemical shifts. Although interresidual C$^{\beta}$ peaks show up very weakly in the refocused hC$^{\alpha}$hNH only, they can be observed in the non-refocused experiment reasonably well in most cases. Seeking high sensitivity for C$^{\beta}$, the unrefocused experiment (*red*) presented shows truncation artefacts in the ^{13}C dimension, most notably for the C$^{\alpha}$ resonances, which are of higher intensity. See Fig. 3c for assessing the maximum obtainable resolution. The refocused hC$^{\alpha}$hNH and the unrefocused hC^{x}hNH were recorded within 2.5 and 2d using 4 and 8 ms t_{1max} and 100 Hz exponential and −10 Hz Gaussian multiplication (with a shift of the bell by 0.2), respectively, for ^{13}C. An indirect evolution to 14 ms and Gaussian multiplication of −10 Hz with a bell shift of 0.1 for ^{15}N and 35 Hz exponential broadening for ^{1}H were used for both experiments. Weak signals as shown with a *grey box* are below the lowest contour chosen. Due to the undirected nature of dipolar transfers, weak non-sequential correlations are found in most strips in addition to the desired peaks

effects (see pulse programs in Fig. 1b, d), introduces a signal loss of 31% as measured in the first increment (shown in Fig. 4b).

$^{1}H/^{15}N$ separated 3D correlations were recorded for the entire ^{13}C bandwidth without refocusing and for ^{13}CO and for $^{13}C^{ali.}$ with refocusing of $^{1}J_{CaCO}$. Figure 5 shows strip plots representing the sequential walk along the backbone for aliphatic carbons for a representative subset of residues of the α-spectrin SH3 domain.

In contrast to scalar transfers, signal to noise obtained for the dipolar based experiments can be expected not to depend on ^{15}N transverse relaxation times T_2 and thus be widely independent of the kind of target protein. On the other hand, the loss of magnetization during out-and-back scalar N/C transfers (similar for C/C transfers, if neglecting the evolution of passive couplings) can be shown to significantly depend on T_2. This loss corresponds to a) an exponential decay with $T_2(^{15}N)$ during a duration t_{max} reflecting the evolution of maximum achievable antiphase magnetization with respect to transverse relaxation and b) incomplete evolution of the antiphase component in this interval:

$$I(t_{max}, T_2) \propto (\sin \pi J t_{max})^2 e^{-2t_{max}/T_2} \quad (1)$$

and

$$t_{max} = \frac{1}{\pi J} \arctan(\pi J T_2), \quad (2)$$

with $I(t_{max}, T_2)$ denoting the obtained intensity after a complete out-and-back scalar N/C-transfer and T_2 denoting echo $T_2(^{15}N)$.

The relation (2) for t_{max}, the duration of one INEPT step to be used for maximal efficiency, was obtained analytically from setting $\frac{dI(t)}{dt} = 0$. This compromise between relaxation and evolution (or reconversion) of NC antiphase terms (with approximately 11 and 7 Hz for $^{1}J_{NC\alpha}$ and $^{2}J_{NC\alpha}$, respectively) (Bax and Ikura 1991), results in roughly between 20 (calculated value for 10 ms $T_2(^{15}N)$ and 68 ms (calculated value for a $T_2(^{15}N)$ of 50 ms) transverse ^{15}N magnetization. (Linser et al. 2008, 2011b) Alike, 12–14 ms transverse $^{13}C^{\alpha}$ magnetization ($^{1}J_{C\alpha-CO} = 55$ Hz and $^{1}J_{C\alpha C\beta} = 35$ Hz) in total represent a typical duration of the relay step in scalar HNCACO and HNCACB experiments (Linser et al. 2010a, 2011b). Relaxation during transverse carbon magnetization on C^{α} can roughly be considered as $T_{2eff}(^{13}C^{\alpha}) = 7.5$ ms and less sample dependent due to dominant evolution of $^{1}J_{C\alpha C\beta}$, which is difficult to refocus. (Linser et al. 2010a) Figure 6 delineates this behaviour for proteins with shorter ^{15}N T_2, as obtained from equation (1), displaying the obtained signal intensities for the current preparation (T_2 (^{15}N) = 22 ms) in conjunction with a calculated extrapolation towards shorter ^{15}N T_2. Transverse relaxation times obtained for non-crystalline proteins previously (Linser et al. 2011b) are denoted. Evidently, for ^{15}N T_2 times getting shorter, scalar transfer-based experiments become increasingly difficult, which makes the strategy presented here a more and more feasible alternative for resonance assignment. Supplementary Figure 5 represents similar plots for intra- and interresidual CO and intra- and interresidual C^{β} correlations. There the relative performance of dipolar versus scalar transfers is lower due to the larger $^{1}J_{NCO}$ favouring the INEPT transfer and the long distance H^N-C^{β} decreasing the HC transfer efficiency, respectively.

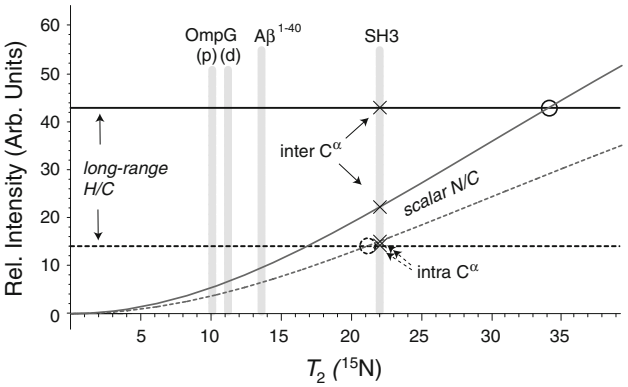

Fig. 6 ^{15}N T_2 dependence of alternative scalar transfers. For proteins with a short effective ^{15}N transverse relaxation time T_2, scalar transfers result in loss of magnetization through relaxation during $^{15}N/^{13}C$ INEPTs. Long-range H/C transfers on the other hand are not sensitive to ^{15}N T_2. *Crosses* mark relative signal intensities obtained for representative residues from 3D triple-resonance experiments based on long-range H/C transfers ($hC^{x}hNH$, *horizontal lines*) and based on scalar transfers (HNCA, *curves*), respectively. *Circles* denote the theoretical T_2 of similar s/n for the scalar and dipolar HNC correlations. *Solid* and *dashed lines* reflect intra- and interresidual correlations, respectively. Values for the Outer membrane protein G (OmpG) are displayed as measured for protonated (p) and deuterated lipids (d). T_2 values taken from (Linser et al. 2011b)

Conclusion

Proton detection, which is feasible for sample preparation providing dilute protonation in exchangeable sites, has been shown to enable triple-resonance assignment experiments employing magnetization transfer by virtue of scalar couplings. For cases with less favourable transverse relaxation times of the involved heteronuclei, scalar transfers result in large relaxation losses. This work presents a way towards proton-detected $^{1}H/^{15}N/^{13}C$ correlations relying on long-range $^{1}H/^{13}C$ dipolar transfers instead. This strategy is shown to correlate the backbone amide group with carbon shifts of various kinds, including intra- and interresidual CO, C^{α}, and C^{β}, providing valuable information for resonance assignment and thereby not relying on long T_2 (^{15}N). Whereas the obtained correlations potentially involve the complete ^{13}C spectral range, $^{1}J_{CaCO}$-refocused experiments

selecting either carbonyls or aliphatic carbons provide a higher resolution. The presented approach can be considered a valuable alternative to dipolar experiments providing too few ^{13}C shifts per residue and to scalar experiments in cases where short heteronuclear T_2 would be detrimental for the achievable signal to noise.

Acknowledgments I am grateful to Prof. Bernd Reif for the generous gift of the protein material. Dr. James Hook is kindly acknowledged for his support to the project. This research was financed by the Analytical Centre, UNSW.

References

Agarwal V, Diehl A, Skrynnikov N (2006) High resolution 1H detected 1H, 13C correlation spectra in MAS solid-state NMR using deuterated proteins with selective 1H, 2H isotopic labeling of methyl groups. J Am Chem Soc 128:12620–12621

Agarwal V, Linser R, Fink U, Faelber K, Reif B (2010) Identification of hydroxyl protons, determination of their exchange dynamics, and characterization of hydrogen bonding by MAS solid-state NMR spectroscopy in a microcrystalline protein. J Am Chem Soc 132:3187–3195

Akbey Ü et al (2009a) Optimum levels of exchangeable protons in perdeuterated proteins for proton detection in MAS solid-state NMR spectroscopy. J Biomol NMR 46:67–73

Akbey Ü, Oschkinat H, van Rossum B (2009b) Double-nucleus enhanced recoupling for efficient 13C MAS NMR correlation spectroscopy of perdeuterated proteins. J Am Chem Soc 131: 17054–17055

Akbey Ü, Camponeschi F, van Rossum B-J, Oschkinat H (2011) Triple resonance cross-polarization for more sensitive 13C MAS NMR spectroscopy of deuterated proteins. ChemPhysChem doi: 10.1002/cphc.201100084:

Asami S, Schmieder P, Reif B (2010) High resolution 1H-detected solid-state NMR spectroscopy of protein aliphatic resonances: access to tertiary structure information. J Am Chem Soc 132: 15133–15135

Bax A, Ikura M (1991) An efficient 3D NMR technique for correlating the proton and ^{15}N backbone amide resonances with the a-carbon of the preceding residue in uniformly $^{15}N/^{13}C$ enriched proteins. J Biomol NMR 1:99–104

Cady SD et al (2010) Structure of the amantadine binding site of influenza M2 proton channels in lipid bilayers. Nature 463:689–692

Castellani F et al (2002) Structure of a protein determined by solid-state magicangle-spinning NMR spectroscopy. Nature 420:98–102

Chevelkov V, Rehbein K, Diel A, Reif B (2006) Ultra-high resolution in proton solid-state NMR spectroscopy at high levels of deuteration. Angew Chem Int Ed 45:3878–3881

Emsley L, Bodenhausen G (1990) Gaussian pulse cascades: new analytical functions for rectangular selective inversion and in-phase excitation in NMR. Chem Phys Lett 165:469–476

Franks WT, Kloepper KD, Wylie BJ, Rienstra CM (2007) Four-dimensional heteronuclear correlation experiments for chemical shift assignment of solid proteins. J Biomol NMR 39:107–131

Franks WT et al (2008) Dipole tensor-based atomic-resolution structure determination of a nanocrystalline protein by solid-state NMR. Proc Natl Acad Sci USA 105:4621–4626

Goddard TD, Kneller DG (2004) SPARKY 3. University of California, San Francisco

Heise H et al (2005) Molecular-level secondary structure, polymorphism, and dynamics of full-length a-synuclein fibrils studied by solid-state NMR. Proc Natl Acad Sci USA 102:15871–15876

Hiller M et al (2005) Solid-state magic-angle spinning NMR of outer-membrane protein G from *Escherichia coli*. ChemBioChem 6:1679–1684

Huang KY, Siemer AB, McDermott AE (2011) Homonuclear mixing sequences for perdeuterated proteins. J Magn Reson 208:122–127

Huber M et al (2011) A proton-detected 4D solid-state NMR experiment for protein structure determination. ChemPhysChem 12:915–918

Lange A et al (2006) Toxin-induced conformational changes in a potassium channel revealed by solid-state NMR. Nature 440:959–962

Lewandowski JR et al (2011) Enhanced resolution and coherence lifetimes in the solid-state NMR spectroscopy of perdeuterated proteins under ultrafast magic-angle spinning. J Phys Chem Lett 2:2205–2211

Linser R (2011) Side-chain to backbone correlations from solid-state NMR of perdeuterated proteins through combined excitation and long-range magnetization transfers. J Biomol NMR 51:221–226

Linser R, Chevelkov V, Diehl A, Reif B (2007) Sensitivity enhancement using paramagnetic relaxation in MAS solid-state NMR of perdeuterated proteins. J Magn Reson 189:209–216

Linser R, Fink U, Reif B (2008) Proton-detected scalar coupling based assignment strategies in MAS solid-state NMR spectroscopy applied to perdeuterated proteins. J Magn Reson 193:89–93

Linser R, Fink U, Reif B (2010a) Narrow carbonyl resonances in proton-diluted proteins facilitate NMR assignments in the solid state. J Biomol NMR 47:1–6

Linser R, Fink U, Reif B (2010b) Assignment of dynamic regions in biological solids enabled by spin-state selective NMR experiments. J Am Chem Soc 132:8891–8893

Linser R, Bardiaux B, Higman V, Fink U, Reif B (2011a) Structure calculation from unambiguous long-range amide and methyl 1H–1H distance restraints for a micro-crystalline protein with MAS solid state NMR. J Am Chem Soc 133:5905–5912

Linser R et al (2011b) Proton detected solid-state NMR of fibrillar and membrane proteins. Angew Chem Int Ed 50:4508–4512

Loquet A et al (2008) 3D Structure determination of the Crh protein from highly ambiguous solid-state NMR restraints. J Am Chem Soc 130:3579–3589

McDermott AE, Creuzet FJ, Kolbert AC, Griffin RG (1992) High-resolution magic-angle-spinning NMR spectra of protons in deuterated solids. J Magn Reson 98:408–413

Nielsen JT et al (2009) Unique identification of supramolecular structures in amyloid fibrils by solid-state NMR spectroscopy. Angew Chem Int Ed 48:2118–2121

Opella SJ, Marassi FM (2004) Structure determination of membrane proteins by NMR spectroscopy. Chem Rev 104:3587–3606

Paravastu AK, Leapman RD, Yau WM, Tycko R (2008) Molecular structural basis for polymorphism in Alzheimer's ß-Amyloid fibrils. Proc Natl Acad Sci USA 47:18349–18354

Pauli J, Baldus M, van Rossum B, de Groot H, Oschkinat H (2001) Backbone and side-chain 13C and 15 N signal assignments of the a-spectrin SH3 domain by magic angle spinning solid-state NMR at 17.6 Tesla. ChemBioChem 2:272–281

Pervushin KV, Wider G, Wüthrich K (1998) Single transition-to-single transition polarization transfer (ST2-PT) in [^{15}N, ^{1}H]-TROSY. J Biomol NMR 12:345–348

Petkova AT et al (2002) A structural model for Alzheimer's ß-amyloid fibrils based on experimental constraints from solid state NMR. Proc Natl Acad Sci USA 99:16742–16747

Schanda P, Huber M, Verel R, Ernst M, Meier BH (2009) Direct detection of $^{3h}J_{NC}$, hydrogen-bond scalar couplings in proteins

by solid-state NMR spectroscopy. Angew Chem Int Ed 48:9322–9325

Schanda P, Meier BH, Ernst M (2010) Quantitative analysis of protein backbone dynamics in microcrystalline ubiquitin by solid-state NMR spectroscopy. J Am Chem Soc 132:15957–15967

Siemer AB et al (2006) Observation of highly flexible residues in amyloid fibrils of the HET-s prion. J Am Chem Soc 128:13224–13228

Vranken WF et al (2005) The CCPN data model for NMR spectroscopy: development of a software pipeline. Proteins 59:687–696

Wasmer C et al (2008) Amyloid fibrils of the HET-s(218–289) prion form a beta solenoid with a triangular hydrophobic core. Science 319:1523–1526

Zhou DH et al (2007a) Proton-detected solid-state NMR spectroscopy of fully protonated proteins at 40 kHz magic-angle spinning. J Am Chem Soc 129:11791–11801

Zhou DH et al (2007b) Solid-state protein structure determination with proton-detected triple resonance 3D magic-angle spinning NMR spectroscopy. Angew Chem Int Ed 46:8380–8383